Understanding the Effect of Functional Groups on the Seeded Growth of Copper on Carbon Nanotubes for Optimizing Electrical Transmission

Kourtney D. Wright,[†] Cathren E. Gowenlock,[‡] Joseph C. Bear,[§] and Andrew R. Barron*[‡, †, ξ]

[†] Department of Chemistry, Rice University, Houston, TX 77005, USA.

[‡] Energy Safety Research Institute (ESRI), Swansea University Bay Campus, Fabian Way, Swansea, SA1 8EN, UK.

[§] Department of Chemistry, University College London, 20 Gordon Street, London, WC1H 0AJ, UK.

[ξ] Department of Materials Science and Nanoengineering, Rice University, Houston, Texas 77005, USA.

ABSTRACT: We present a study of the seeded growth of copper on the surface of two classes of single-walled carbon nanotubes (SWNTs) in order to compare the effects of surface functional groups. Pyridine functionalized HiPco SWNTs and ultra-short SWNTs (US-SWNTs) were synthesized (py-SWNTs and py-US-SWNTs, respectively) and the functionality used as seed sites for copper, *via* an aqueous electroless deposition reaction, as a comparison to carboxylic acid functionality present on piranha etched SWNTs and the native US-SWNTs. UV-visible spectroscopy demonstrated the take-up of Cu(II) ions by the functionalized SWNTs. TEM showed that the SWNTs with pyridine functionality more rapidly produced a more even distribution of copper seeds with a narrower size distribution (3-12 nm for py-US-SWNTs) than those SWNTs with oxygen functional groups (ca. 30 nm), showing the adventitious role of

pyridine functional group in the seeding process. Seed composition was confirmed as Cu(0) by XPS and SAED. Copper growth rate and morphology were shown to be affected by degree of pyridine functionality, the length of the SWNT and the electroless reaction solvent used.

INTRODUCTION

Most of power distribution today is *via* the electrical grid, which relies on copper (or aluminum) cables within an iron sheath. Unfortunately, over 10% of the power transmitted is lost due, in the main, to resistive heating effects within the cables. To compensate for each 200 MW of line loss, another coal plant must be on-line. In 2011, summertime electrical generation in the US was 1,026 GW. Therefore, a 10% loss would be equivalent to *ca*. 200 average-sized coal power plants. In addition to issues associated with power loss, the weight of any conductor has a significant impact on energy consumption. This is particularly true in the automotive and aerospace industries.[1]

Proposed long term solutions to low transmission losses of electricity involve carbon nanotubes (CNTs), in particular metallic single walled carbon nanotubes (SWNTs),[2,3] or high temperature superconducting materials.[4] Both of these approaches have significant technical challenges to be overcome; however, a near term solution involves the improvement in conductivity and ampacity of copper by the addition of CNTs, resulting in a Cu-CNT composite material termed ultra-conductive copper.[5-7] The fabrication of such composites has been accomplished in a variety of different ways including electrolytic co-deposition,[8,9] powder metallurgy,[10,11] powder injection molding,[12] and electroless plating.[13,14] One of the best

performing Cu-CNT composites was reported by Subramaniam et $al.$,[7] showing a conductivity of 4.7 x 10^5 S/cm and an ampacity of 630 x 10^6 A/cm^2, which is a 100 fold increase in the ampacity of the Cu-CNT composite versus Cu. Although the reported ampacity[7] may be artificially high due to heat transfer from the short test structure (50 μm) to the contacts and the substrate,[15] we were interested in their Cu growth method nonetheless. They reported that the Cu was grown on the CNTs in a two-step process: organic electroplating of seed particles followed by aqueous electroplating to create the bulk.[7] They proposed that a controlled homogeneous seeding of Cu onto the surface is key to their results,[7] suggesting that an understanding of the factors that control this seeding process are important in controlling the Cu-CNT composite formation, and hence its performance.

Careful study of the protocol reported by Subramaniam et $al.$[7] shows that they also appear to pre-coordinate Cu(II) ions to the CNTs presumably via sidewall functional groups.[16] It is well known that as prepared and after purification CNTs have significant sidewall functionality,[17,18] and since the main influence of the CNTs (in Cu-CNT) is to reduce the temperature coefficient of resistivity as compared to Cu, rather than act as additional conduction pathways,[7,19] sidewall purity would not be expected to be important. In fact in the wide range of Cu-CNT studies, no special care was taken in purifying the CNTs with regard to functional groups. The goal of this study was to understand the effect of different functional group on the seeded growth of Cu on the CNTs.

A commonly used approach to facilitate the deposition of Cu nanoparticles on CNTs is through oxidation of the CNTs to graft epoxide, hydroxyl, and carboxyl groups on the surface.[20-22] We have also shown that functionalization with pyridine, phosphines, and thiols of CNTs can be achieved in a number of ways and this allows for coordination of metal ions, compounds or

nanoparticles.[23-27] Of these substituents, pyridine functionality not only acts as an efficient ligand,[24,28,29] but also facilitates a decrease in the copper reduction potential, resulting in the preferential reduction of the surface bound Cu(II) to Cu(I).[29-35] This coordinated Cu can then act as a catalyst for the deposition of further Cu(II) ions from solution, allowing controlled seeded growth by electroless deposition.[28,29,36] In the case of CNTs, we have reported that pyridine (py) functionalization may be achieved through 1,3-dicyclohexylcarbodiimide (DCC) coupling of isonicotinic acid (with CNT-OH groups) or 4-hydroxypyridine (with CNT-CO_2H groups).[24]

Based upon the forgoing, we proposed a study to understand and control the seeded growth of Cu on functionalized CNTs in order to synthesize templates for subsequent Cu growth. In the present study, we have investigated two classes of CNTs: acid purified HiPco SWNTs and oxidized ultra-short SWNTs (US-SWNTs). The latter have lengths <100 nm and extensively oxidized sidewalls, including carboxylic groups.[37-39] In the study we contrast the difference between Cu seeded on pyridine functionalized and carboxylic acid functionalized CNTs; to our knowledge there is no prior study of pyridine functionality in the Cu seeding of CNTs, although we have reported pyridine versus hydroxyls activation on alumina surfaces.[28] The comparison between py-functionalized SWNTs (py-SWNTs) and py-functionalized US-SWNTs (py-US-SWNTs) allows for the effects of the concentration of the functional groups (*i.e.*, py:C ratio) to be studied.

EXPERIMENTAL SECTION

Materials and Methods. All reagents were purchased from Sigma Aldrich Ltd. and used as received unless otherwise noted. 4-Hydroxypyridine was dried over sulfuric acid for 2 days in a vacuum desiccator before use. Oxidized US-SWNTs were donated by the Wilson group at Rice University and were placed under vacuum for an hour before use. Raw HiPco SWNTs, 09-

4

HiPco-0093 batch No. 195.7, were obtained from the Carbon Nanotube Laboratory (CNL) at Rice University and used as received.

X-ray photoelectron spectra (XPS) were recorded on a PHI Quantera XPS Scanning Microprobe using a monochromated Al-K_α X-ray source (1486.7 eV). All spectra were recorded using a charge neutralizer to limit differential charging and subsequently calibrated to the carbon peak at a binding energy of 284.5 eV. Survey scans were recorded at a pass energy of 140 eV and high-resolution data at a pass energy of 26 eV. Data was fitted using MultiPak software. Transmission electron microscopy (TEM) images were recorded using a Jeol 1230 High Contrast TEM with a W filament and an operating voltage of 80 kV or using a Jeol 2100 TEM with a field emission electron gun and an operating voltage of 200 kV. TEM samples were prepared by drop-drying a dilute solution of carbon nanotubes suspended in ethanol onto a 300-mesh gold grid with a lacey carbon film (Agar-Scientific Ltd). Selective area diffraction (SAED) patterns and electron dispersive X-ray (EDS) spectra were acquired using a Jeol 2100 TEM with a field emission electron gun and an operating voltage of 200 kV. UV-visible absorption spectra were acquired using Cary 100 and Agilent 8453 UV-visible spectrophotometers, scanning between 550 and 900 nm with a step size of 0.5 nm. ^{1}H nuclear magnetic resonance (NMR) experiments were performed on a Bruker 400 MHz instrument in D_2O at 25 ˚C. Thermogravimetric analysis (TGA) was carried out using a TA Instruments SDT Q600 thermo-gravimetric analyzer. All samples for TGA were purged for 1 h then ramped at 10 ˚C/min to 100 ˚C, where they remained for 1 h under 100 mL/min flow of argon. For TGA experiments run in argon, the temperature was then ramped at 10 ˚C/min to 1000 ˚C. For TGA experiments run in air, the gas was switched to air with a 100 mL/min flow rate and the samples were held at 100 ˚C for another 5 min. Then, the temperature was ramped at a rate of 10 ˚C/min to 1100 ˚C. Raman spectra were recorded on

a Renishaw InVia confocal Raman spectrometer with the exciting wavelength at 532 nm and a 50x objective lens.

Synthesis of Piranha-Etched SWNTs. Raw HiPco SWNTs were purified by a method adapted from the literature.[40] Raw HiPco SWNTs (100 mg) were oxidised in wet air at 225 °C for 18 h, followed by sonication in hydrochloric acid (37 %, 300 mL) for 15 mins to remove metal catalyst particles. The SWNTs were then filtered over a PTFE filter, washed several times with deionized water and finally annealed in argon at 800 °C for 1 h. These purified SWNTs were then piranha-etched using a method adapted from the literature.[24] Room temperature piranha solution (4:1, vol/vol 96 % H_2SO_4/30 % H_2O_2) was added to purified SWNTs (1 mL piranha/1 mg of nanotubes) and stirred for 60 mins. The oxidation was then quenched by a twenty-fold dilution with deionized water, followed by filtration over a polycarbonate filter, washing with deionized water until pH neutral and finally washing with ethanol. The resulting piranha-etched SWNTs were dried *in vacuo*.

Synthesis of US-SWNT-COCl. This method was adapted from the literature.[24] Oxidized US-SWNTs (30 mg) were added to a Schlenk flask under argon with anhydrous dimethylformamide (DMF, 0.3 mL) and thionyl chloride (7.25 mL). The suspension was stirred at 60 ˚C for 48 h under argon. Dichloromethane was added to bring the total volume to *ca*. 25 mL. After decanting off excess solvent, the functionalized US-SWNTs were dried *in vacuo* then stored under argon.

Synthesis of Py-US-SWNT. This method was adapted from the literature.[24] Hydroxypyridine (90 mg) and US-SWNT-COCl (30 mg) were added to a Schlenk flask under argon with dichloromethane (25 mL). The suspension was stirred at 50 ˚C for 48 h under argon,

6

and then the product was filtered over a PTFE filter and washed with dichloromethane and ethanol. Finally the py-US-SWNTs were dried *in vacuo*.

Synthesis of Py-SWNT. This method was adapted from the literature.[24] DCC (269 mg), 4-hydroxypyridine (126 mg) and 4-dimethyl-aminopyridine (DMAP, 12 mg) were dissolved in methanol (10 mL) and piranha-etched SWNTs (100 mL, 200 mg.L^{-1}) in methanol were added to the solution. The suspension was stirred at 50 ˚C for 48 h, and then the product was filtered over a PTFE filter and washed with methanol. Finally the py-SWNTs were dried *in vacuo*.

UV-Visible Study of Divalent Copper Adsorption by Py-US-SWNTs and Py-SWNTs. Py-US-SWNTs or Py-SWNTs (10 mg) were bath sonicated in methanol (4 mL) for 10 mins, followed by addition of copper nitrate hemi(pentahydrate) (7.4 mg) in methanol (2 mL), a further 10 mins sonication and finally 24 hours of rotary shaking. The resulting suspension was then filtered and the filtrate analyzed using UV-Vis spectroscopy (λ_{max}=790nm).

Functionalization of Py-US-SWNTs and US-SWNTs with Copper Seeds. This method was adapted from the literature using 1/8 of the original reagent concentrations.[36] An aqueous room-temperature solution (42 mL) of Py-US-SWNTs (12.9 mg), $CuSO_4 \cdot 5H_2O$ (62 mg) and ethylenediaminetetraacetic acid (EDTA, 47 mg) was bath sonicated for 10 mins, then hydrazine (78%, 0.15 mL) was added dropwise whilst stirring. Aliquots of solution were removed, filtered and rinsed with deionized water after 2, 5, 10, 15 and 30 mins of reaction time and then dried *in vacuo*.

Preparation of Pyridine-Capped Seeds for ^{1}H NMR Spectroscopy. Hydrazine (0.22 mL) was added dropwise to a stirred aqueous solution (42 mL) of $CuSO_4 \cdot 5H_2O$ (90 mg) and EDTA (70 mg). Once bubbling had stopped, the product was filtered and placed in a D_2O

solution of pyridine (3.5 mL and 0.35 mL, respectively) to form an orange-brown solution which was filtered and analyzed by ^{1}H NMR and TEM.

RESULTS AND DISCUSSION

Characterization of Py-SWNTs and Py-US-SWNTs. Pyridine functionalized HiPco SWNTs and US-SWNTs were prepared according to modifications of previously reported methods (Figure 1).[24]
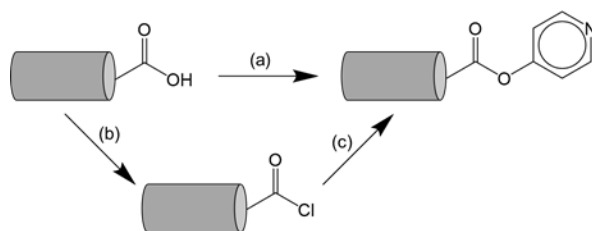
Figure 1. Schematic of the two synthetic routes to pyridine-functionalized SWNTs using 4-hydroxypyridine/DCC/DMAP in MeOH (a) for HiPco SWNTs or for US-SWNTs (b) SOCl$_2$/DMF followed by (c) 4-hydroxypyridine in CHCl$_3$ (c).

SEM analysis of HiPco SWNTs confirmed their length as *ca*. 2-3.5 μm (Figure S1, Supporting Information), whilst TEM analysis of US-SWNTs confirmed their length as less than 100 nm and their width as 1-2 nm (Figure S2, Supporting Information). After cleaning by wet oxidation and HCl washing, TEM analysis of HiPco SWNTs showed the presence of small unevenly shaped particles (*ca*. 3-8 nm), which, given the presence of Fe in the XPS (see below), are likely to be residue from the iron catalyst used in the HiPco process. Furthermore, after piranha-etching and py-functionalization, some unevenly shaped small particles are still present, albeit heterogeneously distributed across the sample.

In contrast to the HiPco SWNTs, TEM analysis of py-US-SWNTs does not show any significant concentration of nanoparticles, suggesting that the Fe catalyst residue (from the HiPco SWNTs from which the US-SWNTs are made) is removed during the synthesis of US-SWNTs.[37,38,41,42] This is confirmed by the lack of Fe in the XPS spectrum, although the residue observed in the TGA (see below) suggests that some (1.3% w/w) catalyst residue is present.

TGA of piranha-etched SWNTs and py-SWNTs in air (Figure S3, Supporting Information) show weight loss due to functional groups coinciding with the pyrolysis of the SWNTs. The residue in each case is the oxidized catalyst residue.[43-45] Comparing the initial weight loss beginning at 200 °C, the py-SWNTs show a more drastic weight decrease than the piranha-etched SWNTs. This is consistent with the presence of additional functional groups.[37-39] This is confirmed by the TGA in argon (Figure S3, Supporting Information), where the total weight loss by 800 °C can be attributed to the loss of the functional groups to leave un-functionalized SWNTs and the catalyst residue.[46] By 800 °C, the purified SWNTs, piranha-etched SWNTs, and py-SWNTs lose 7.2%, 24.7% and 32.7% respectively. This is consistent with increasing functionality from mild oxidation during purification (epoxides[18]), to more aggressive oxidation during piranha-etching (carboxylic acid groups[47]), and to pyridine functionalization.[24] The TGA analysis in air of oxidized US-SWNTs and py-US-SWNTs (Figure S3, Supporting Information) shows the weight percent beginning to drop from around 200 °C due to the pyrolysis of functional groups. In the case of py-US-SWNTs, there is increased weight loss in this region, indicating that pyridine groups were added to the US-SWNTs (c.f., Figure 1) in agreement with the XPS data below. There is a final drop in weight beginning at 500 ˚C corresponding to the combustion of US-SWNTs. The residue remaining at 800 ˚C only contributes 1.4% w/w to the US-SWNT samples, indicating a very small residual catalyst content. This is consistent with

XPS data, which did not indicate any significant Fe content (see below). The TGA in argon of the US-SWNT samples shows an increase in weight loss by 800 °C from 20.3% to 24.8% w/w from loss of functional groups from the oxidized US-SWNTs and py-US-SWNTs, respectively, indicating that the oxidized US-SWNTs were functionalized with pyridine groups.

XPS analysis of the purified SWNTs shows an O:C ratio of 1:12.9 which increases to 1:6.9 for the piranha-etched SWNTs (Table 1), consistent with significant sidewall functionalization having taken place. XPS analysis of py-SWNTs and py-US-SWNTs both show the presence of nitrogen, confirming the functionalization with pyridine substituents (Table 1). If it is assumed that all of the oxygen present on the samples is in the form of carboxylic acid groups (-CO_2H) and that all of these become functionalized upon reaction (Figure 1) then a N:O ratio of 1:2 is expected. However, the observed ratio for py-SWNTs is 1:9.7, while for py-US-SWNTs the ratio is 1:7.1. The lower N:O ratios suggest that either the reaction is incomplete or that much of the O content is associated with non-carboxylic acid functionality. An explanation for this would be that more of the oxygen signal in the py-SWNT could be due to sidewall epoxide groups, consistent with previous studies which show that supposedly purified SWNTs can contain significant epoxide substitution.[18] The N:C ratio represents a measure of the number of pyridine functional groups per unit length of the CNT. As such, the ratio for py-SWNTs is lower (1:73.0) than that for py-US-SWNTs (1:38.8), showing that the ultra-short tubes contain a greater amount of pyridine functionality than the sample derived from piranha-etched SWNTs.

Table 1. XPS analysis with atomic composition (%) and element ratios for purified and functionalized SWNTs.

Sample	C (%)	O (%)	N (%)	Fe (%)	N:C ratio	O:C ratio	N:O ratio
purified SWNT	92.8	7.2	0.0	0.0	n/a	1:12.9	n/a
Piranha-etched SWNT	86.1	12.5	0.0	1.4	n/a	1:6.9	n/a
py-SWNT	86.9	11.6	1.2	0.3	1:73.0	1:7.5	1:9.7
US-SWNT	87.5	12.5	0.0	0.0	n/a	1:7.0	n/a
py-US-SWNT	82.8	15.0	2.2	0.0	1:38.8	1:5.4	1:7.1

The O1s XP spectra of piranha-etched SWNTs and US-SWNTs may be deconvoluted to multiple oxygen species attributable to carboxylic acid groups, epoxides, hydroxyls, and carbonyl groups groups (Figure S4, Supporting Information). Deconvoluted oxygen peaks for piranha-etched SWNTs are slightly shifted compared to those for US-SWNTs, with the shift being due to peak broadening attributable to charging.[48] The ratio of oxygen atoms in the carbonyl groups to carbon atoms for piranha-etched SWNTs and US-SWNTs is 1:72 and 1:42, respectively. This would suggest a higher carboxylic acid functionality content in US-SWNTs, which is consistent with the higher pyridine functionality. Indeed, these ratios are very similar to the N:C ratios in Table 1, suggesting that most of the carboxylic acid groups are functionalized with pyridine. In fact, from the composition, it is possible to determine that for both pyridine functionalized samples the N:carboxylic acid ratio is *ca*. 1:1, suggesting both a high conversion and uniform reactivity for both of the two pyridine functionalization methods used. The deconvolution of the appropriate O1s XP spectra show peaks due to epoxides, hydroxyls, and carbonyl groups, but the peak due to carboxylic acid groups observed for the precursors

disappears, consistent with pyridine functionalization (Figure S5, Supporting Information). With regard to the Fe content observed in Table 1, it was found that the XPS results varied depending on the area analyzed, indicating inhomogeneity across the samples. In addition, residual catalyst is often encapsulated with amorphous carbon, resulting in a lower Fe signal than expected from TGA. For these reasons, and the low percentage of Fe that is present in the samples, it is difficult to give a meaningful error estimate for the Fe composition. TGA was therefore used to more accurately determine bulk Fe content.

Raman spectra of the purified SWNTs compared to the raw HiPco SWNTs showed a 2.4 times increase in the G band intensity corresponding to removal of carbonaceous materials during the cleaning process (Figure S6, Supporting Information). This G band intensity increases by a further 10 % after piranha-etching of the SWNTs, indicating that carbonaceous material is continuing to be removed during the etching process. The G/D band intensity ratios of the purified SWNTs, piranha-etched SWNTs and pyridine functionalized SWNTs were 6.1, 6.2 and 5.5 respectively, indicating that there is not a significant change in the number and distribution of sidewall defects on piranha-etching and pyridine functionalization, but as confirmed by XPS only the nature of the functional groups has changed.

Cu(II) Binding to Functionalized SWNTs. To test the efficacy of copper ions binding to py-SWNT and py-US-SWNT before they are reduced to zero-valent copper, we investigated their reaction with a standard solution (0.016 M copper nitrate; see Experimental). As a comparison, carboxylic acid functionalized SWNTs (US-SWNTs and piranha-etched SWNTs) were also investigated. The presence of a binding reaction between the SWNTs and the copper ions is reflected by a drop in the UV-visible absorbance (λ_{max} = 790nm) for all of the reaction solutions as a function of time. Based upon the final absorbance intensities at t = 24 hours

12

(Figure S7, Supporting Information), the adsorption of copper (mg Cu/g SWNT) may be calculated (Table 2). These results show that copper ions have a good interaction with the pyridine functional groups, ensuring that the copper seeds will be bound to those groups upon reduction. The oxidised SWNTs (piranha-etched SWNTs and US-SWNTs) showed a higher absorption of copper than their pyridine functionalised SWNT counterparts, which may be attributed to the multiplicity of oxygen species that can bind the Cu(II), or the greater steric bulk of the pyridine functionality hindering binding.[49,50]

Table 2. Weight of copper ions absorbed from a standard divalent copper solution by SWNTs.

| Sample	Cu adsorption (mg Cu/g SWNT)
Purified SWNT	0.5
Piranha-Etched SWNTs	14.2
py-SWNT	8.0
US-SWNT	14.7
py-US-SWNT	7.3

Seeded Growth of Cu(0) on Py-US-SWNTs Versus US-SWNTs. Given the low catalyst content in the py-US-SWNTs and the higher concentration of pyridine functional groups per C, the seeded growth of Cu on py-US-SWNTs was investigated first. Copper was seeded onto the py-US-SWNT pyridine groups using electroless plating,[36] with hydrazine as reducing agent (Eq. 1) and EDTA as complexing agent for the Cu(II) ions. To determine the best method for Cu seed growth and to understand how different parameters affect the size and quantity of the seeds, a time and concentration study was conducted (Table 3).

$$CuSO_4 + N_2H_4 \rightarrow Cu + N_2 + H_2SO_4 \tag{1}$$

The initial trial (**1** in Table 3) employed the same reagent concentrations as a method reported in the literature for Cu growth on isonicotinic acid functionalized alumina,[28,29,36] and the reaction was allowed to proceed until gas evolution stopped. This results in the formation of large (>100 nm) agglomerated cubic particles sparsely distributed across the sample (Figure 2). Unfortunately, no growth is observed on the majority of the py-US-SWNTs. This suggests that the reduction of copper is happening too quickly, i.e., once an initial seed occurs, grain growth occurs rapidly. It is also possible to observe some smaller Cu NPs (*ca*. 35 nm), see Figure 2.

Table 3. The quantities of reagents used per liter of deionized water in three different trials of copper electroless plating on py-US-SWNTs.

Trial	Py-US-SWNT (g/L)	$CuSO_4 \cdot 5H_2O$ (g/L)	EDTA (g/L)	Hydrazine (mL/L)
1	0.31	11.84	8.96	28.56
2	0.31	8.88	6.72	21.42
3	0.31	1.48	1.12	3.57
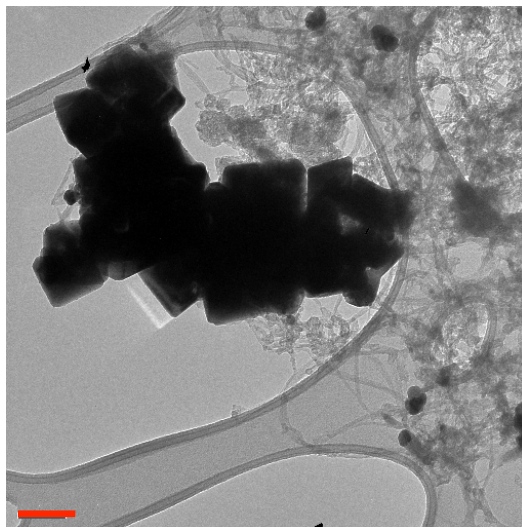
Figure 2. TEM image of Cu crystals grown on py-US-SWNTs by electroless deposition using trial **1** (Table 3) Scale bar = 100 nm.

With a view to reducing the reaction rate, the reagent concentrations were reduced to ¾ of their original quantities (**2** in Table 3) and the reaction was run for 5, 10, 15 and 30 minutes. The TEM images in Figure 3 show large agglomerated cubic crystals of Cu for all four reactions times (diameter = 120 - 225 nm), with the prevalence of cubes increasing with time. However, the occurrence of the desired small Cu spheres increased overall relative to the higher concentration reaction and increases with increasing reaction time (Figure 3d).
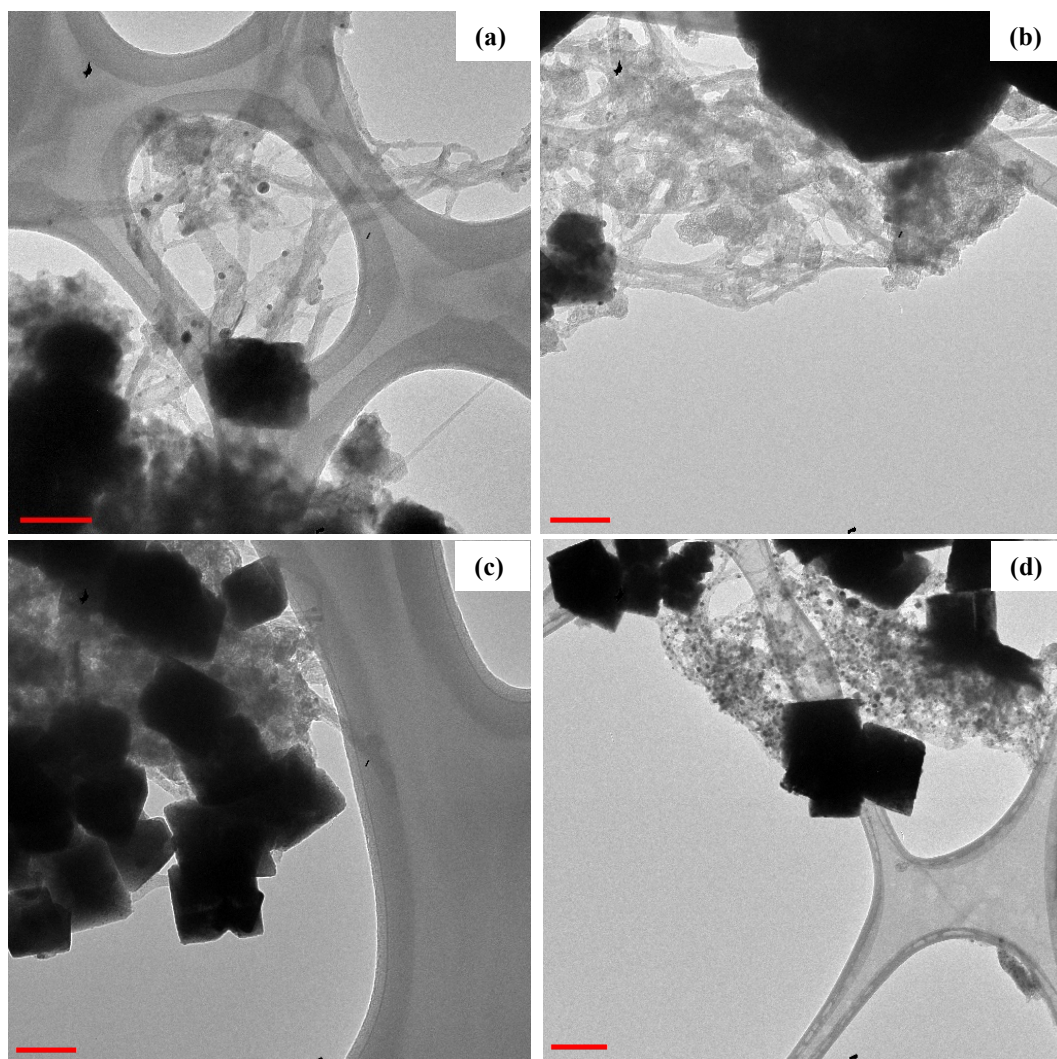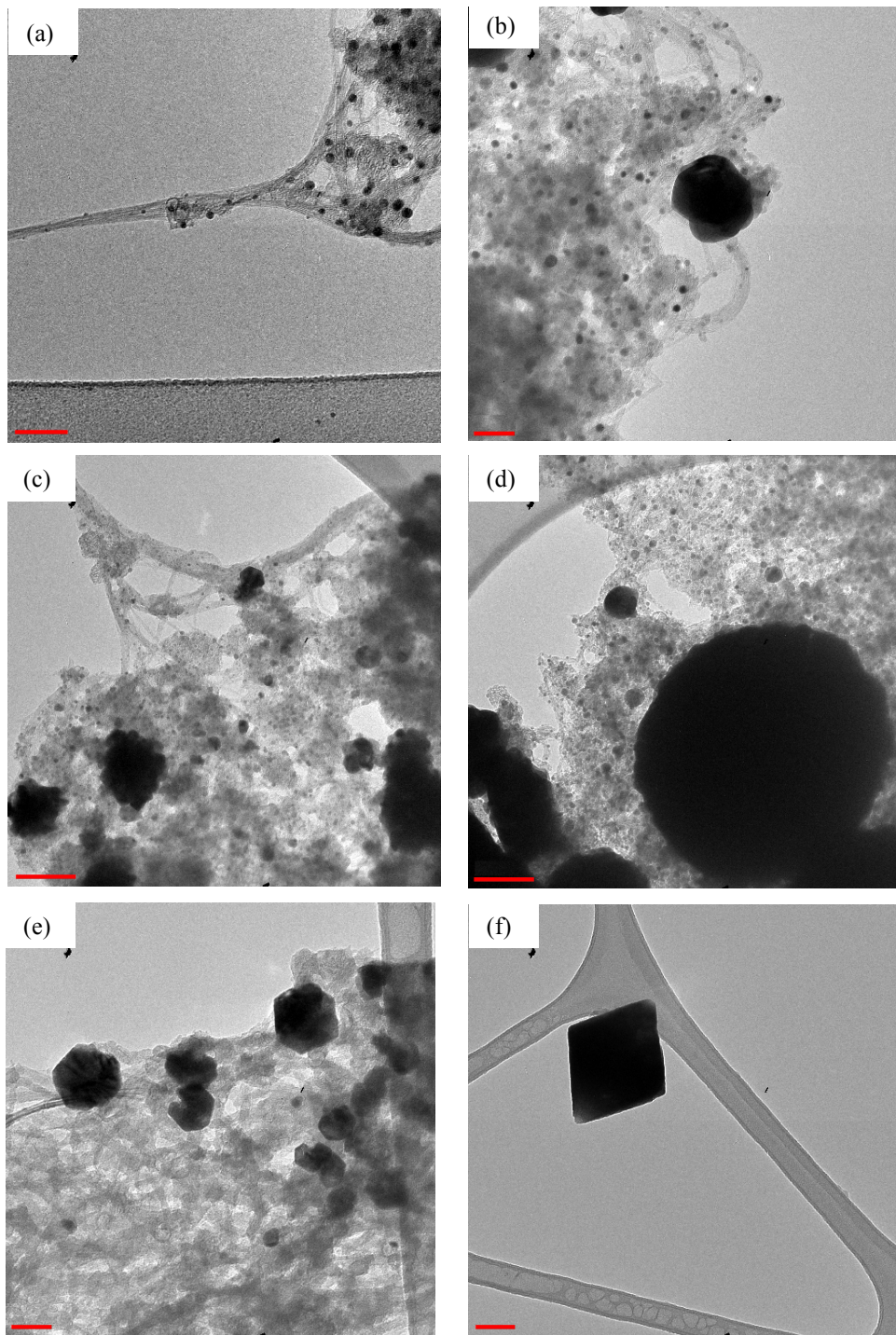
Figure 3. TEM images of the electroless deposition of copper onto py-US-SWNTs using trial **2** in Table 3 for (a) 5 min, (b) 10 min, (c) 15 min, and (d) 30 min of reaction time. Scale bars are 100 nm (a, b, c) and 200 nm (d).

In order to eliminate the large cubes and maximize the small spheres, the reaction was run with $^1/_8$ of the original reagent concentrations for 2, 5, 10, 15 and 30 minutes (**3** in Table 3). The TEM images in Figure 4 show the growth of many of the desired seed particles, which range in size

from 3 – 12 nm for reaction times up to 15 minutes. However, beginning at 5 minutes (Figure 4b), larger (>50 nm) spherical particles begin to grow. At 30 minutes, the particles become hexagonal or square in shape, and many of them are not associated with SWNTs at all (Figure 4f), suggesting homogeneous crystal growth rather than seeded growth. Additionally, there are very few small spherical particles present after 30 minutes, which may be due to Ostwald ripening.[51] Therefore, to obtain small copper seeds on the SWNTs, the ideal reagent concentrations are $^1/_8$ the reported literature concentrations[36] and the ideal reaction time is 2 minutes. The resulting material meets the requirements of a uniform dispersion of seeded Cu NPs on the surface of the SWNTs without significant homogeneous nucleation.

Figure 4. TEM images of the electroless deposition of copper onto py-US-SWNTs using trial **3** in Table 3 for (a) 2 min, (b) 5 min, (c) 10 min, (d) 15 min and (e and f) 30 min of reaction time. Scale bars are (a, b, e) 50 nm and (c, d, f) 100 nm.

The selected area electron diffraction (SAED) pattern (Figure S9, Supporting Information) for copper seeded SWNTs after 2 mins of growth (Figure 4a) gave a pattern assignable to 111, 200, 220, and 311 atomic planes and corresponding to a face-centered cubic (FCC) lattice structure.[52] A calculated lattice parameter of 3.6 Å combined with the FCC lattice structure, confirms the diffraction pattern is from zero-valent copper metal.[52] Furthermore, the SAED leaves little doubt that the observed particles are not from copper oxide, iron, or iron oxides from residual catalyst material because these species have very different lattice structures; CuO has a monoclinic structure,[53] zero-valent iron has a body-centered cubic structure[52] and, under ambient conditions, iron(III) oxide has a rhombohedral or cubic spinel structure.[54] Therefore, the particles shown in the TEM image in Figure 4 are confirmed to be zero-valent copper, which is in agreement with the XPS data below.

TGA was used to determine how much Cu was added to the py-US-SWNTs. In this regard, the 2 min and 30 min products were analyzed by TGA in air, such that the residue should represent Cu (oxide) only. In agreement with the TEM images (Figure 4a and e), the results in Figure 5 clearly show an increase in copper with increased reaction time. Comparing these results with those from the UV-visible Cu(II) adsorption experiment (above), more copper was seeded onto the tubes in the 2 min electroless deposition (~220 mg Cu/g py-US-SWNTs) than was adsorbed on the py-US-SWNTs (7.3 mg Cu/g py-US-SWNT). This is expected, since the functional groups on the electroless deposited py-US-SWNTs are bound to seeds that contain many atoms, while the functional groups in the UV-visible experiment are presumably bound to single copper ions. Doing a similar comparison for the 30 min electroless deposition shows that 2.6 times more copper was deposited on py-US-SWNTs compared to the 2 min reaction. However, as discussed previously, the TEM image in Figure 4e shows sparse coverage of the py-US-SWNTs with large

copper particles for the 30 min reaction time. Thus, there are not necessarily more pyridine groups bound by Cu but, rather, there are just larger Cu particles. The TGA results in Figure 5 show the onset of combustion starting around 200 °C which continues until about 400 °C. Compared to the data for py-US-SWNTs, the range of combustion is shifted down by 200 °C. We suspect that this is due to the combustion catalytic activity of the copper.[55] A steady weight percent is reached at 400 °C for the 2 minute reaction and at 500 °C for the 30 minute reaction. At this point, the only species left to contribute to the weight percent is copper oxides (assuming negligible residual catalyst content).
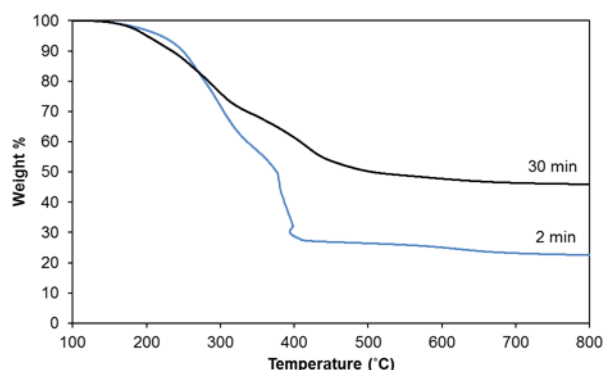
Figure 5. TGA in air of Cu-py-US-SWNTs prepared using trial **3** (Table 3) for 2 min and 30 min of reaction time.

The XPS analysis of Cu-py-US-SWNT confirms the presence of copper for the 2, 5, 10, 15 and 30 min reaction times (Table 4). The amount of Cu increases from 2 to 5 min of reaction time. However, reaction times between 5 and 15 min show similar Cu content, and the 30 min reaction time shows a decrease in Cu. These Cu percentages reflect that XPS is a surface technique, and

the location of analysis is crucial. Greater weight should therefore be placed on the TGA results, which as a bulk technique clearly show an increase in Cu content with reaction time.

**Table 4. XPS analysis and element ration for Cu seeded py-US-SWNTs.**

Reaction time (mins)	C (%)	O (%)	N (%)	Cu (%)
2	74.0	18.8	2.3	4.9
5	73.6	18.1	1.6	6.6
10	72.1	19.7	1.8	6.5
15	72.8	18.8	1.8	6.6
30	74.3	19.1	2.3	4.2

In agreement with the SAED data, deconvolution of the high resolution Cu $2p_{3/2}$ XPS signal for the 2 min reaction gave a 91-93% Cu(0) contribution to the overall Cu signal (932.4 eV).[56] The remaining signal was consistent with CuO (933.8 eV),[56] which is presumably on the particle surface. The amount of CuO increases for the 30 min reaction time, resulting in a slightly lower Cu(0) content at 86%.

We have shown that with the correct choice of reaction time and reagent concentration, py-US-SWNTs can be decorated with seed crystals of Cu(0). ^{1}H NMR spectroscopy was used to investigate whether the copper seeds were bound to the pyridine functional groups. Free Cu particles in solution were used to determine Cu's interaction with pyridine in Cu-py-US-SWNTs. The copper particles were synthesized according to trial **3** in Table 3, but without the presence of py-US-SWNTs. The particles were filtered and mixed with a D_2O solution of pyridine, causing the particles to dissolve and generating a clear, brown-orange solution. This solution was filtered

and the ^{1}H NMR spectrum of the resulting filtrate compared to that of pyridine, where the peaks in the presence of the Cu NPs are shifted downfield and are broadened as compared to the spectra of pyridine, while TEM confirms that copper nanoparticles were present in the NMR sample (Figure S10, Supporting Information).

In order to determine the effect that the pyridine functional groups have on Cu morphology, oxidized US-SWNTs were deposited with Cu using the optimized method for py-US-SWNTs (**3** in Table 3). As the TEM images in Figure 6 show, deposition on oxidized US-SWNTs results in the formation of Cu particles with a wider size distribution than those on py-US-SWNTs. After 2 minutes of reaction time, there is a clear difference between the seed growth on US-SWNTs (Figure 6a) and seed growth on py-US-SWNTs (Figure 4a). Growth on py-US-SWNTs shows small Cu seeds of a narrow size distribution (3-12 nm) well distributed across the py-US-SWNTs (Figure 4a). In contrast, seed growth on US-SWNTs results in Cu particles that are comparatively large (~30 nm) and also agglomerated (Figure 6a). Beginning at 5 min (Figure 6b), even larger particles (~100 nm) grow and become more closely packed with increasing reaction time (Figure 6b-d). After 30 minutes, large agglomerated particles are seen, but square particles are also formed (Figure 6e). Although large amorphous particles are also seen after 5 minutes of reaction time in the presence of py-US-SWNTs, they are much more abundant on the oxidized US-SWNTs. Further, small Cu seeds (2.5-5 nm) on oxidized US-SWNTs only occurred intermittently at all reaction times and did not seem to grow in size with deposition time (see, Figure 6f for a representative image). On the contrary, py-US-SWNTs showed uniform copper seed deposition between 2 and 15 min of reaction time (Figure 4a-d). These results show that pyridine functional groups are crucial to the formation of well dispersed Cu seeds with a narrow size distribution (after 2 min) on SWNTs.
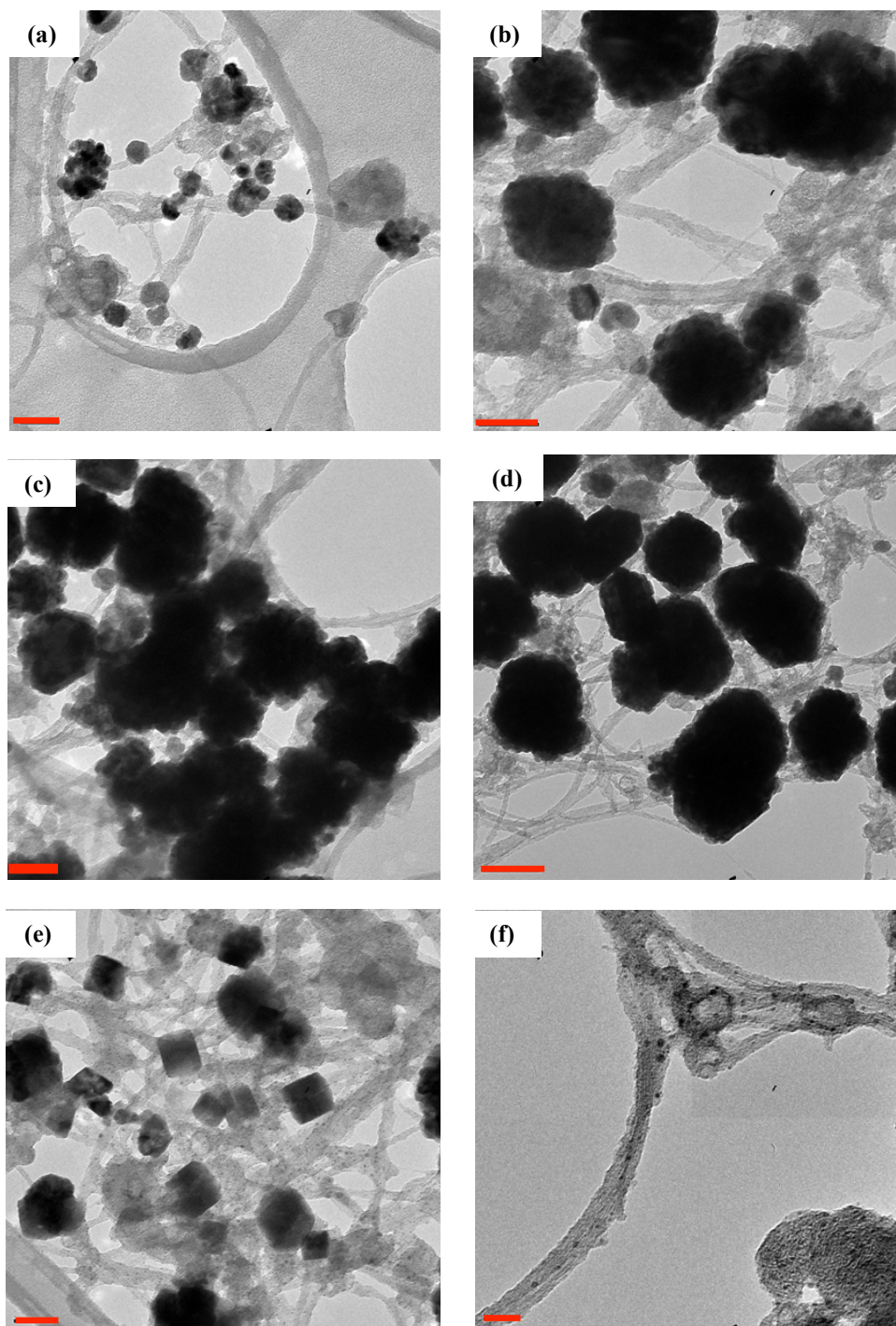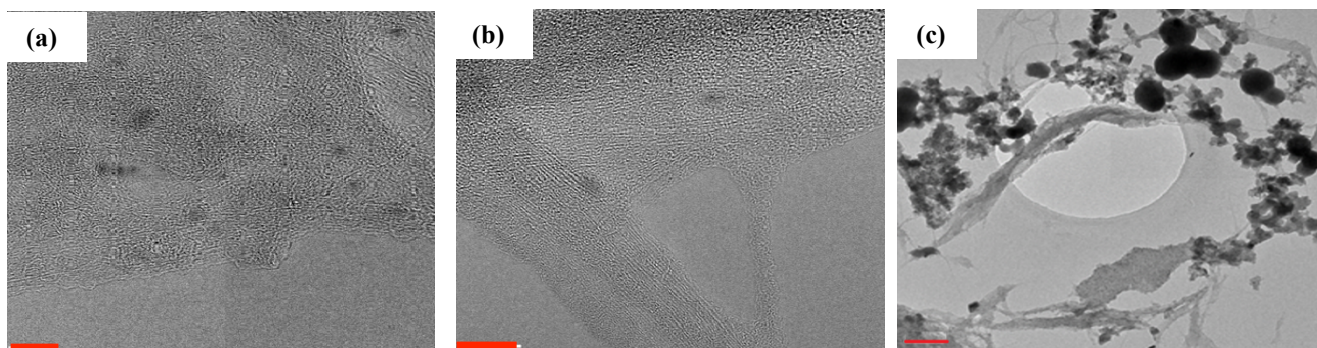
Figure 6. TEM images of the electroless deposition of copper onto US-SWNTs using trial **3** (Table 4) showing large particle growth at (a) 2 min, (b) 5 min, (c) 10 min, (d) 15 min and (e) 30 min of reaction time and (f) some intermittent seed growth at all reaction times. Scale bars are (a, b, c, e) 50 nm, (d) 100 nm and (f) 20 nm.

Seeded Growth of Cu(0) on Py-SWNTs Versus Piranha-Etched SWNTs. Given the success of the aqueous electroless deposition results with py-US-SWNTs, the first trial conducted with py-SWNTs was also in aqueous medium with the same reagent concentrations as the optimized method for py-US-SWNTs (Table 3), as shown in **4** of Table 5. After 2 min of reaction time, the TEM image of the resulting sample showed a uniform dark staining of the py-SWNTs (Figure 7a) compared to unreacted py-SWNTs (Figure 7b). They also showed irregularly shaped particles that are typical of residual catalyst material. The stained appearance suggests that Cu is deposited in a very uniform manner along the entire length of the py-SWNTs. However, as the appearance of a TEM image can change depending on how over- or under-focused it is, the presence of Cu was also confirmed by energy dispersive X-ray spectroscopy (EDS) mapping of the surface of py-SWNT after 2 min Cu deposition (Figure 8).

Table 5. The quantities of the reagents used per liter of solvent in two different trials of copper electroless plating on py-SWNTs.

Trial	Py-SWNT (g/L)	CuSO$_4$·5H$_2$O (g/L)	EDTA (g/L)	Hydrazine (mL/L)	Solvent
4	0.31	1.48	1.12	3.57	H$_2$O
5	1.73	84.07	-	25.38	MeOH

Figure 7. TEM images of (a) the electroless deposition of copper onto py-SWNTs using trial **4** (Table 5) for 2 min of reaction time, (b) py-SWNTs and (c) the electroless deposition of copper onto py-SWNTs using trial **4** for 30 min of reaction time, showing large particles of copper and clusters of small copper seeds. Scale bars are (a, b) 10 nm and (c) 100 nm.
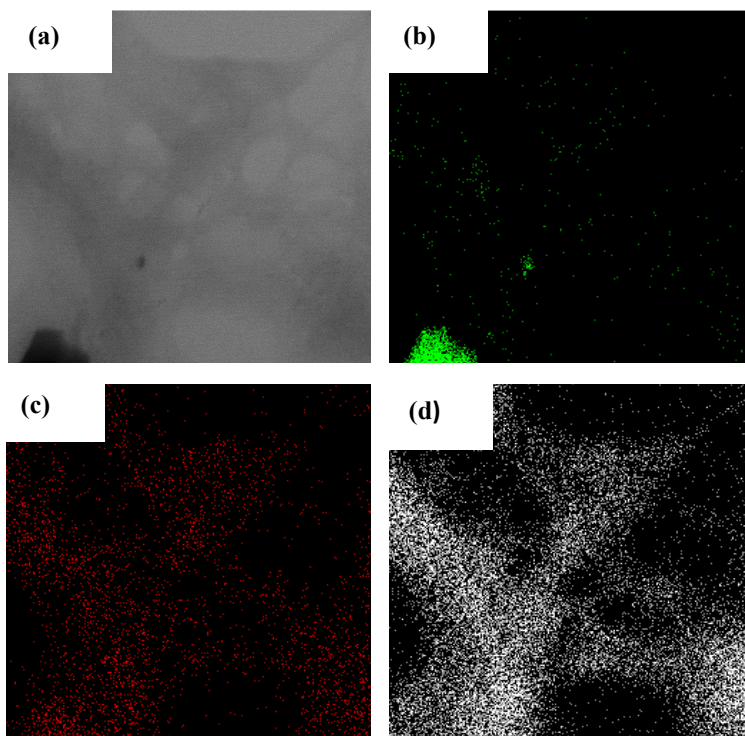

Figure 8. STEM image (a) and associated EDS maps of (b) Fe, (c) Cu and (d) C of a sample of py-SWNT after electroless deposition of copper using trial **4** (Table 5) for 2 min of reaction time.

The Cu K$_\alpha$ EDS map (Figure 8c) shows copper distributed over the entire surface of the sample, consistent with the dark staining of the py-SWNTs seen in Figure 7a. Furthermore, the defined particles seen in TEM images are confirmed to be catalyst material by the Fe K$_\alpha$ EDS map (Figure 8b). For comparison, EDS mapping was also used to characterize unreacted py-SWNTs, however in this instance the Cu K$_\alpha$ signal was evenly dispersed across the entire map area including in regions of vacuum and hence can be attributed to scattered X-rays from the Cu sample holder. These results confirm that Cu deposition on py-SWNT with short reaction times results in a highly uniform coating of Cu across the SWNT surface.

When the reaction is allowed to proceed for 30 min, large spherical particles are then formed as well as small nanoparticle seeds of Cu (Figure 7c). The small seeds show a similar morphology to the copper seeds obtained with py-US-SWNT after 2 and 5 min reaction times (Figure 4a and b). However, this result suggests that while a uniform distribution of Cu onto the SWNT surface is the initial result, either not all these act as potential seeds or, once a seed grows, Ostwald ripening results in a small number of larger crystals growing.

The above results for the aqueous deposition of Cu on SWNTs shows a clear difference in the rate at which the Cu particles form on the HiPco nanotubes compared to similar depositions on US-SWNTs. Although this may be the result of a combination of factors such as tube length and degree of pyridine functionality, we also suspected that the low dispersibility of SWNTs in water might play a role in this as well. For this reason, a second trial (**5** in Table 5) of electroless deposition of copper on the py-SWNTs was conducted in MeOH to aid suspension of the py-SWNTs. Because EDTA showed low solubility in MeOH, it was omitted from the reaction. After 30 mins of electroless deposition, the TEM image showed a dark coating over the surface of the py-SWNTs (Figure 9a), similar to that observed in the aqueous deposition (Figure 7a).

There was also the presence of small nanoparticles (Figure 9b), but these are likely due to Fe rather than Cu seeds given their irregular shape and the EDS results above (Figure 8).
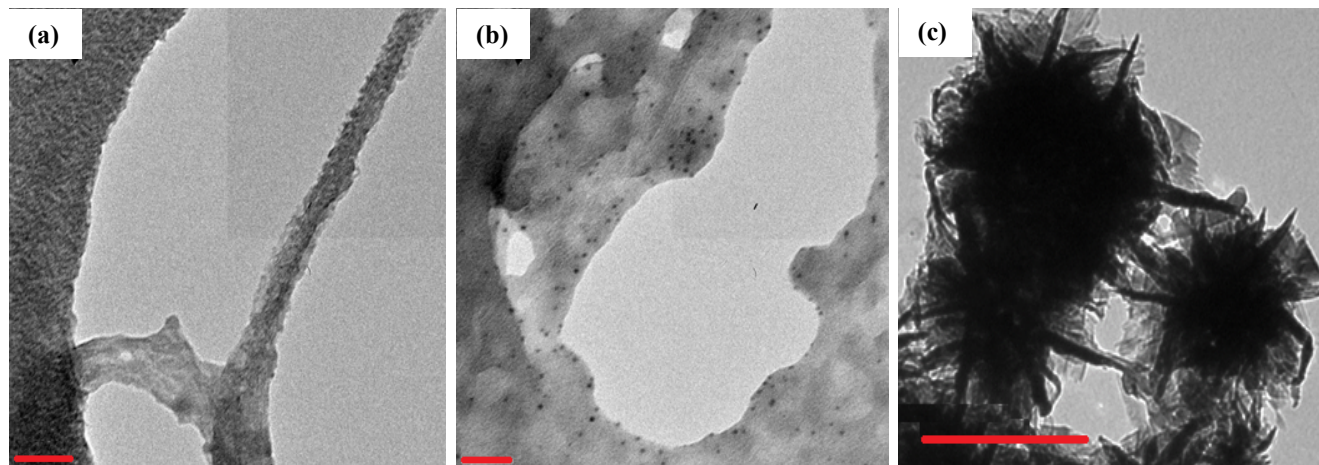
Figure 9. TEM images of (a) the electroless deposition of copper onto py-SWNTs using trial **5** (Table 5) for 30 min of reaction time, showing SWNTs with a dark coating and (b) residual catalyst particles; and (c) the electroless deposition of copper onto py-SWNTs using trial **5** (Table 5) for 24 h of reaction time, showing the growth of 'sea urchin' type structures. Scale bars are (a, b) 20 nm and (c) 500 nm.

When the electroless deposition proceeded for 24 h, eventually the copper growth formed 'sea urchin' type structures (Figure 9c). Although the concentration of the SWNTs and $CuSO_4 \cdot 5H_2O$ are higher than any of the US-SWNT trials, it is interesting that the morphology of the Cu is vastly different from that with extended growth using py-US-SWNTs. Furthermore, the 30 minute deposition in MeOH with higher $CuSO_4 \cdot 5H_2O$ and without Cu(II)-complexing EDTA resulted in the same Cu morphology as the 2 minute aqueous reaction. Because the 30 minute

aqueous reaction showed the presence of large particles and Cu seeds, it seems that the MeOH actually reduces the reaction rate or alters the solubility/reactivity of the py-SWNTs.

To determine how much copper has been grown on the py-SWNTs, the 2 min and 24 h electroless deposition products were analyzed by TGA in air (Figure S11, Supporting Information). Residues at the end of the TGA analysis can be attributed to copper and iron oxides, with the 24 h sample clearly showing a greater residue than the 2 min sample, in agreement with the TEM images.

Electroless deposition of copper was also carried out on piranha-etched SWNTs to determine the efficacy of deposition in the absence of pyridine functionality, using the optimized method **4** in Table 5. Deposition of copper on piranha-etched SWNTs after 2 and 5 mins reaction time resulted in a similar uniform dark staining (Figure 10a) to that seen for deposition on py-SWNTs (Figure 7a), however by 30 mins reaction time the TEM image in Figure 10b shows the growth of the desired copper seed particles, ranging in size from 2-10 nm. Additionally, there are also larger (35-60 nm) agglomerated copper particles present. Although the copper seed particles are not evenly distributed across the piranha-etched SWNTs, their distribution is less patchy than those seen on the py-SWNT sample (Figure 7c), and there are more of them. This improved seeding at 30 mins reaction time for piranha-etched SWNTs compared to py-SWNT can be attributed to the greater ease of dispersion of piranha-etched SWNTs in an aqueous medium compared to py-SWNT. Despite the benefits brought about by the greater ease of dispersion, seeding with piranha-etched SWNTs does not exclusively give small copper seeds at 30 reaction time; larger (35-60 nm) particles are also present. This contrasts with seeded growth with py-SWNTs where evenly dispersed small seeds of a small size distribution (3-12 nm) can be

obtained. Carboxylic acid and other oxygen functional groups therefore do not give the controlled seeding that pyridine groups on well-dispersed SWNTs are capable of producing.
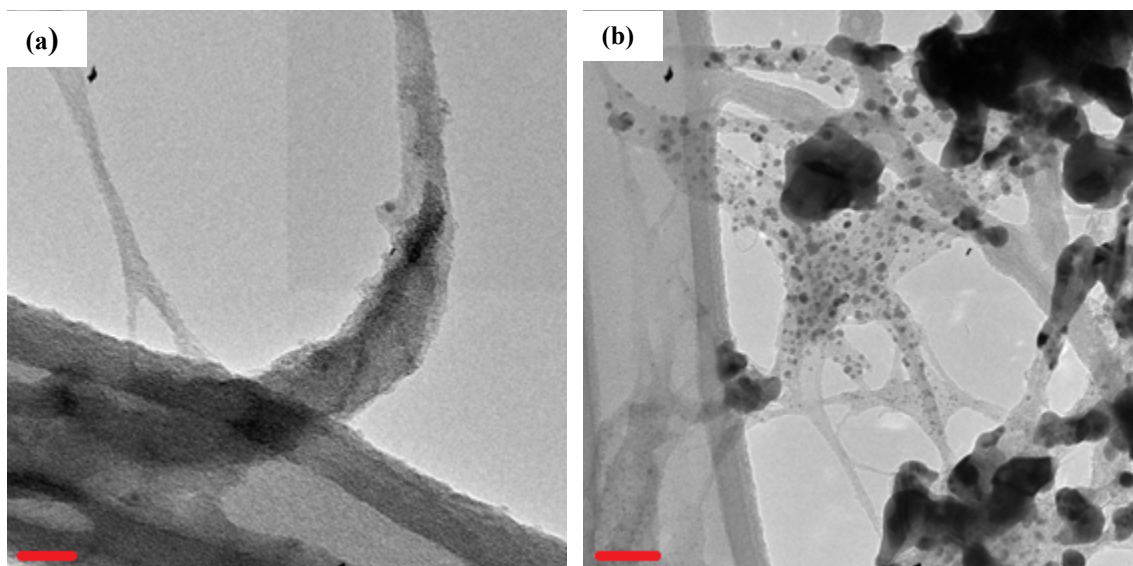
Figure 10. TEM images of the electroless deposition of copper onto piranha-etched SWNTs using trial **4** in Table 5 for (a) 2 min and (b) 30 min of reaction time. Scale bars are (a) 20 nm and (b) 50 nm.

CONCLUSIONS

The goal of this study was to understand the effects of different functional groups on the process of seeding Cu on CNTs. The Cu seeded CNTs have applications in Cu-CNT composite fabrication,[7] for which electrical properties offer an interim solution to power distribution.[57-59] Pyridine functionalized SWNTs and US-SWNTs were synthesized and functionalized with copper seeds, and contrasted with piranha-etched SWNTs and native carboxylic acid US-SWNTs. XPS analysis of the samples showed that US-SWNTs contain a higher atomic % of carboxylic acid groups and, correspondingly, the py-US-SWNTs contain a higher concentration of pyridine groups as compared to the piranha-etched SWNTs and py-SWNTs. A UV-visible

spectroscopy experiment showed that Cu(II) ions are taken up by py-functionalized SWNTs and US-SWNTs, confirming the ions' interaction with the pyridine groups. After optimization of reaction time and concentration, 3-12 nm Cu seeds were deposited uniformly on py-US-SWNTs. These were confirmed as Cu(0) by XPS and SAED. A ^{1}H NMR study showed that free copper seeds are capped by pyridine groups, indicating that the seeds are indeed bound to the pyridine groups on py-US-SWNTs and py-SWNTs. A comparison of Cu deposition using the optimized method on py-US-SWNTs and oxidized US-SWNTs indicated that the pyridine groups are critical to the formation of evenly dispersed Cu seed particles with a small size distribution. However, using the same 2 min optimized protocol with py-SWNTs resulted in the observation of dark coatings on the tubes in TEM, suggesting the formation of small Cu clusters on the tubes. This was verified using EDS mapping, which showed a uniform layer of Cu across the py-SWNTs. The reduced rate of Cu seeding on py-SWNTs compared to py-US-SWNTs is likely due to their lower dispersibility, but tube length and a decreased level of pyridine functionalization may play a part. However, when a higher $CuSO_4$ concentration was used without EDTA in MeOH for 30 min of deposition time, the py-SWNTs were deposited with a dark coating of Cu similar to the optimized aqueous 2 min reaction. Given the higher Cu(II) concentration, lack of Cu(II)-complexing EDTA and increased reaction time, these results are unexpected. Despite better dispersion of py-SWNTs in MeOH, our results suggest that it slows the Cu deposition rate. Allowing the MeOH solution to proceed for 24 h resulted in large 'sea urchin' type structures. These results suggest that the length of the SWNT and/or the degree of pyridine functionality, as well as the choice of solvent, all have an effect on Cu growth rate and morphology.

ASSOCIATED CONTENT

Supporting Information

   The Supporting Information is available free of charge on the http://pubs.acs.org. SEM and TEM images of HiPco SWNT and US-SWNT denoting their dimensions. TGA of piranha-etched SWNT, py-SWNT, US-SWNT and py-US-SWNT. High resolution O1s XP spectra. Raman spectra of raw and purified HiPco SWNT. UV-visible spectra of copper solutions filtered from US-SWNT, py-US-SWNT, piranha-etched SWNT and py-SWNT. Schematic of copper electroless deposition reaction. SAED pattern of the electroless deposition of copper onto py-US-SWNT. ^{1}H NMR spectra of pyridine-capped Cu NPs. TGA of py-SWNT after electroless deposition of copper.

AUTHOR INFORMATION

Corresponding Author

*E-mail: a.r.barron@swansea.ac.uk; arb@rice.edu (A.R.B)

Author Contributions

The manuscript was written through contributions of all authors. All authors have given approval to the final version of the manuscript.

Notes

The authors declare no competing financial interest.

ACKNOWLEDGMENTS

REFERENCES

(1)   Baur, J.; Silverman, E. Challenges and Opportunities in Multifunctional Nanocomposite Structures for Aerospace Applications. *MRS Bull*. **2007**, *32* (4), 328–334.

(2)   McEuen, P. L.; Fuhrer, M. S.; Park, H. K. Single-Walled Carbon Nanotube Electronics. *IEEE Trans. Nanotechnol*. **2002**, *1,* 78–85.

(3)   Jarosz, P.; Schauerman, C.; Alvarenga, J.; Moses, B.; Mastrangelo, T.; Raffaelle, R.; Ridgley, R.; Landi, B. Carbon Nanotube Wires and Cables: Near-Term Applications and Future Perspectives. *Nanoscale* **2011**, *3,* 4542–4553.

(4)   Stemmle, M.; Merschel, F.; Noe M.; Hobl, A. AmpaCity - Installation of Advanced Superconducting 10 kV System in City Center Replaces Conventional 110 kV Cables. *Proc. IEEE Int. Conf. ASEMD* **2013,** 323–326.

(5)   Hjortstam, O.; Isberg, P.; Soderholm, S.; Dai, H. Can we achieve Ultra-Low Resistivity in Carbon Nanotube-Based Metal Composites? *Appl. Phys. A: Mater. Sci. Process*. **2004**, *78,* 1175–1179.

(6)   Lee, D. F.; Burwell, M.; Stillman, H. *Priority Research Areas to Accelerate the Development of Practical Ultra-conductive Copper Conductors*, Oak Ridge National Laboratory, 2015.

(7)   Subramaniam, C.; Yamada, T.; Kobashi, K.; Sekiguchi, A.; Futaba, D. N.; Yumura, M.; Hata, K. One Hundred Fold Increase in Current Carrying Capacity in a Carbon Nanotube-Copper Composite. *Nat. Commun.* **2013**, *4,* 2202.

(8)   Chen, Q. US Patent 7651766 B2, 2010.

(9)   Chai, G.; Sun, Y.; Sun J. J.; Chen, Q. Mechanical Properties of Carbon Nanotube-Copper Nanocomposites. *J. Micromech. Microeng.* **2008**, *18,* 035013.

(10)   Dong, S. R.; Tu, J. P.; Zhang, X. B. An Investigation of the Sliding Wear Behavior of Cu-Matrix Composite Reinforced by Carbon Nanotubes. *Mater. Sci. Eng., A* **2001**, *313,* 83–87.

(11)   Uddin, S. M.; Mahmud, T.; Wolf, C.; Glanz, C.; Kolaric, I.; Volkmer, C.; Höller, H.; Wienecke, U.; Roth S.; Fecht, H.-J. Effect of Size and Shape of Metal Particles to Improve Hardness and Electrical Properties of Carbon Nanotube Reinforced Copper and Copper Alloy Composites. *Compos. Sci. Technol.* **2010**, *70,* 2253–2257.

(12)   Muhsan, A. S.; Ahmad, F.; Mohamed, N. M.; Yusoff, P. S. M. M.; Raza, M. R. Homogeneous Distribution of Carbon Nanotubes in Copper Matrix Nanocomposites Fabricated via Combined Technique. *Nanosci. Nanotechnol. Lett.* **2014**, *6,* 865–874.

(13)   Xu, C.; Wu, G.; Liu, Z.; Wu, D.; Meek, T. T.; Han, Q. Preparation of Copper Nanoparticles on Carbon Nanotubes by Electroless Plating Method. *Mater. Res. Bull.,* **2004**, *39,* 1499–1505.

(14)   Daoush, W. M.; Lim, B. K.; Mo, C. B.; Nam D. H.; Hong, S. H. Electrical and Mechanical Properties of Carbon Nanotube Reinforced Copper Nanocomposites Fabricated by Electroless Deposition Process. *Mater. Sci. Eng., A* **2009**, *513–514,* 247–253.

(15) Wang, X.; Behabtu, N.; Young, C. C.; Tsentalovich, D. E.; Pasquali, M.; Kono, J. High-Ampacity Power Cables of Tightly-Packed and Aligned Carbon Nanotubes. *Adv. Funct. Mater.* **2014**, *24,* 3241–3249.

(16) Kim, K. T.; Cha, S. I.; Gemming, T.; Eckert, J.; Hong, S. H. The Role of Interfacial Oxygen Atoms in the Enhanced Mechanical Properties of Carbon-Nanotube-Reinforced Metal Matrix Nanocomposites. *Small* **2008**, *4,* 1936–1940.

(17) Jafry, H. R.; Whitsitt, E.; Barron, A. R. Silica Coating of Vapor Grown Carbon Fibers. *J. Mater. Sci.* **2007**, *42,* 7381–7388.

(18) Ogrin, D.; Chattopadhyay, J.; Sadana, A. K.; Billups, W. E.; Barron, A. R. Epoxidation and Deoxygenation of Single-Walled Carbon Nanotubes: Quantification of Epoxide Defects. *J. Am. Chem. Soc.* **2006**, *128,* 11322–11323.

(19) Yang, Y. L.; Wang, Y. D.; Ren, Y.; He, C. S.; Deng, J. N.; Nan, J.; Chen, J. G.; and Zuo, L. Single-Walled Carbon Nanotube-Reinforced Copper Composite Coatings Prepared by Electrodeposition under Ultrasonic Field. *Mater. Lett.* **2008**, *62,* 47–50.

(20) Mohan, R.; Shanmugharai, A. M.; Sung Hun, R. An Efficient Growth of Silver and Copper Nanoparticles on Multiwalled Carbon Nanotube with Enhanced Antimicrobial Activity. *J. Biomed. Mater. Res., Part B* **2011**, *96B*, 119-126.

(21) Xu, C.; Wub, G.; Liub, Z.; Wub, D.; Meeka, T. T.; Hanc, Q. Preparation of Copper Nanoparticles on Carbon Nanotubes by Electroless Plating Method. *Mater. Res. Bull.* **2004**, *39,* 1499-1505.

(22) Ang, L. M.; Hor, T. S. A.; Xu, G. Q.; Tung, C. H.; Zhao, S. P.; Wang, J. L. S. Decoration of Activated Carbon Nanotubes with Copper and Nickel. *Carbon* **2000**, *38,* 363-372.

(23) Ogrin, D.; Anderson, R. E.; Colorado R.; Maruyama, B.; Pender, M. J.; Moore, V. C.; Pheasant, S. T.; McJilton, L,; Schmidt, H. K.; Hauge, R. H.; Billups, W. E.; Tour, J. M.; Smalley, R. E.; Barron, A. R. Amplification of Single-Walled Carbon Nanotubes from Designed Seeds: Separation of Nucleation and Growth. *J. Phys. Chem. C* **2007,** *111,* 17804–17806.

(24) Hamilton, C. E.; Ogrin, D.; McJilton, L.; Moore, V. C.; Anderson, R.; Smalley, R. E.; Barron, A. R. Functionalization of SWNTs to Facilitate the Coordination of Metal Ions, Compounds and Clusters. *Dalton Trans.* **2008**, 2937.

(25) Moore, V. C.; McJilton, L. A.; Pheasant, S. T.; Kittrell, C.; Anderson, R. E.; Ogrin, D.; Liang, F.; Hauge, R. H.; Schmidt, H. K.; Tour, J. M.; Billups, W. E.; Barron, A. R.; Smalley, R. E. Controlled Attachment Of Metal Nanoparticles to Single Walled Carbon Nanotubes as a Key Step in Their Seeded Growth and Lengthening. *Carbon* **2010**, *48*, 557-570.

(26) Hamilton, C. E.; Barron, A. R. Phosphene Functionalized Single Walled Carbon Nanotubes. *Main Group Chem.* **2009**, *8*, 275-281.

(27) Ogrin, D.; Anderson, R. E.; Colorado, Jr., R.; Maruyama, B.; Pender, M. J.; Moore, V. C.; Pheasant, S. T.; McJilton, L.; Schmidt, H. K.; Hauge, R. H.; Billups, W. E.; Tour, J. M.; Smalley, R. E.; Barron, A. R. Amplification of Single Walled Carbon Nanotubes from Designed Seeds: Separation of Nucleation and Growth. *J. Phys. Chem. C* **2007**, *111*, 17804-17806.

(28) Gowenlock, C. E.; Gomez, V.; McGettrick, J. D.; Andreoli, E.; Barron, A. R. Surface-Initiated Growth of Copper using Isonicotinic Acid-Functionalized Aluminum Oxide Surfaces. *J. Coat. Technol. Res.* **2017**, *14*, 195–205.

(29) Gowenlock, C. E.; McGettrick, J. D.; McNaughter, P. D.; O'Brien, P.; Dunnill, C. W.; Barron, A. R. Copper-Complexed Isonicotinic Acid Functionalized Aluminum Oxide Nanoparticles. *Main Group Chem.* **2016**, *15*, 1–15.

(30) Lyons, A. M.; Vasile, M. J.; Pearce, E. M.; Waszczak, J. V. Copper Chloride Complexes with Poly(2-Vinylpyridine): Preparation and Redox Properties. *Macromolecules* **1988**, *21*, 3125–3134.

(31) Bowman P. B.; Rogers, L. P. Effect of Metal Ion and Ligand on Thermal Stability of Metal Amine Complexes. *J. Inorg. Nucl. Chem.* **1966**, *28*, 2215–2224.

(32) Weiss, J. F.; Tollin, G.; Yoke, J. T. Reactions of Triethylamine with Copper Halides. II. Internal Oxidation-Reduction of Dichlorobis(triethylamine)copper(II). *Inorg. Chem.* **1964**, *3*, 1344–1348.

(33) Clifton, J. R.; Yoke, J. T. Coordination and oxidation of ethylamine and diethylamine by copper(II) chloride. *Inorg. Chem.* **1968**, *7*, 39–46.

(34) Lincoln, K. M.; Offutt, M. E.; Hayden, T. D.; Saunders, R. E.; Green, K. N. Structural, Spectral, and Electrochemical Properties of Nickel(11), Copper(II), and Zinc(II) Complexes Containing 12-Membered Pyridine- and Pyridol-Based Tetra-aza Macrocycles. *Inorg. Chem.* **2014**, *53*, 1406–1416.

(35) Rawat, S. P.; Choudhary, M. Synthesis, Spectroscopic, and Electrochemical Studies on Some New Copper(II) Complexes Containing 2-[(Z)-Phenyl (Pyridine-2-yl) Methylidene] AminoBenzenethiol and Monodentate Ligands. *Int. J. Inorg. Chem.* **2014**, *2014*, 1–8.

(36) Mondin, G.; Wisser, F. M.; Leifert, A.; Mohamed-Noriega, N.; Grothe, J.; Dörfler, S.; Kaskel, S. Metal Deposition by Electroless Plating on Polydopamine Functionalized Micro- and Nanoparticles. *J. Colloid Interface Sci.* **2013**, *411*, 187–193.

(37) Ashcroft, J. M.; Hartman, K. B.; Mackeyev, Y.; Hofmann, C.; Pheasant, S.; Alemany, L. B.; Wilson, L. J. Functionalization of Individual Ultra-Short Single-Walled Carbon Nanotubes. *Nanotechnology* **2006**, *17*, 5033.

(38) Gu, Z.; Peng, H.; Hauge, R. H.; Smalley, R. E.; Margrave, J. L. Cutting Single-Wall Carbon Nanotubes through Fluorination. *Nano Lett.* **2002**, *2*, 1009–1013.

(39) Jung, A.; Graupner, R.; Ley, L.; Hirsch, A. Quantitative Determination of Oxidative Defects on Single Walled Carbon Nanotubes. *Phys. Status Solidi B* **2006**, *243*, 3217–3220.

(40) Chiang, I. W.; Brinson, B. E.; Huang, A. Y.; Willis, P. A.; Bronikowski, M. J.; Margrave, J. L.; Smalley, R. E.; Hauge, R. H. Purification and characterization of single-wall carbon nanotubes (SWNTs) obtained from the gas-phase decomposition of CO (HiPco process). *J. Phys. Chem. B* **2001**, *105* (35), 8297-8301.

(41) Gizzatov, A.; Hernández-Rivera, M.; Keshishian, V.; Mackeyev, Y.; Law, J. J.; Guven, A.; Sethi, R.; Qu, F.; Muthupillai, R.; da G. Cabreira-Hansen, M.; Willerson, J. T.; Perin, E. C.; Ma, Q.; Bryant, R. G.; Wilson, L. J. Surfactant-Free Gd^{3+}-Ion-Containing Carbon Nanotube MRI Contrast Agents for Stem Cell Labelling. *Nanoscale* **2015**, *7*, 12085–12091.

(42) Zhang, J.; Zou, H.; Qing, Q.; Yang, Y.; Li, Q.; Liu, Z.; Guo, X.; Du, Z. Effect of Chemical Oxidation on the Structure of Single-Walled Carbon Nanotubes. *J. Phys. Chem. B* **2003**, *107*, 3712–3718.

(43) Chiang, I. W.; Brinson, B. E.; Huang, A. Y.; Willis, P. A.; Bronikowski, M. J.; Margrave, J. L.; Smalley. R. E.; Hauge, R. H. Purification and Characterization of Single-Wall Carbon Nanotubes (SWNTs) obtained from the Gas-Phase Decomposition of CO (HiPco Process). *J. Phys. Chem. B* **2001**, *105*, 8297–8301.

(44) Gomez, V.; Irusta, S.; Lawal, O. B.; Adams, W.; Hauge, R. H.; Dunnill, C. W.; Barron, A. R. Enhanced Purification Of Carbon Nanotubes by Microwave and Chlorine Cleaning Procedures. *RSC Adv.* **2016**, *6,* 11895–11902.

(45) Andreoli, E.; Suzuki, R.; Orbaek, A. W.; Bhutani, M. S.; Hauge, R. H.; Adams, W.; Fleming, J. B.; Barron, A. R. Preparation and Evaluation of Polyethyleneimine-Single Walled Carbon Nanotube Conjugates as Vectors for Pancreatic Cancer Treatment. *J. Mater. Chem. B* **2014**, *2*, 4740-4747.

(46) Darabi, H. R.; Tehrani, M. J.; Aghapoor, K.; Mohsenzadeh, F.; Malekfar, R. A New Protocol for the Carboxylic Acid Sidewall Functionalization of Single-Walled Carbon Nanotubes. *Appl. Surf. Sci.* **2012**, 258, 8953–8958.

(47) Datsyuk, V.; Kalyva, M.; Papagelis, K.; Parthenios, J.; Tasis, D.; Siokou, A.; Kallitsis, I.; Galiotis, C. Chemical Oxidation of Multiwalled Carbon Nanotubes. *Carbon* **2008**, *46,* 833–840.

(48) Spevack, P. A.; McIntyre, N. S. A Raman and XPS Investigation of Supported Molybdenum Oxide Thin Films. 1. Calcination and Reduction Studies. *J. Phys. Chem.* **1993**, *97,* 11020-11030.

(49) Tolman, C. A. Steric Effects of Phosphorus Ligands in Organometallic Chemistry and Homogeneous Catalysis. *Chem. Rev.* **1977**, *77,* 313–348.

(50) Brown, T. L.; Lee, K. J. Ligand Steric Properties. *Coord. Chem. Rev.* **1993**, *128,* 89–116.

(51) Voorhees, P. W. The Theory of Ostwald Ripening. *J. Stat. Phys.* **1985**, *38*, 231–252.

(52) Cullity B. D.; Stock, S. R. *Elements of X-Ray Diffraction,* 3rd ed.; Pearson/Prentice Hall: Upper Saddle River, NJ, 2001.

(53) Forsyth, J. B.; Hull, S. The Effect of Hydrostatic Pressure on the Ambient Temperature Structure of CuO. *J. Phys:. Condens. Matter* **1991**, *3*, 5257.

(54) Machala, L.; Tuček, J.; Zbořil, R. Polymorphous Transformations of Nanometric Iron(III) Oxide: A Review. *Chem. Mater.* **2011**, *23*, 3255–3272.

(55) Zhou, J. C.; Wu, D. F.; Jiang, W.; Li, Y. D. Catalytic Combustion of Toluene over a Copper-Manganese-Silver Mixed-Oxide Catalyst Supported on a Washcoated Ceramic Monolith. *Chem. Eng. Technol.* **2009**, *32*, 1520–1526.

(56) Fleisch, T. H.; Mains, G. J. Reduction of Copper Oxides by UV-Radiation and Atomic-Hydrogen Studied by XPS. *Appl. Surf. Sci.* **1982**, *10*, 51–62.

(57) Yoo, J. J.; Song, J. Y.; Yu, J.; Lyeo, H. K.; Lee, S.; Hahn, J. H. Multi-Walled Carbon Nanotube/Nanocrystalline Copper Nanocomposite Film as an Interconnect Material. *IEEE Electron. Compon. Technol. Conf.* **2008**, 1282–1286.

(58) Chai, Y.; Chan, P. C. H.; Fu, Y.; Chuang, Y. C.; Liu, C. Y. Copper/Carbon Nanotube Composite Interconnect for Enhanced Electromigration Resistance. *IEEE Electron. Compon. Technol. Conf.* **2008**, 412–420.

(59) Xu, G.; Zhao, J.; Li, S.; Zhang, X.; Yong, Z.; Li, Q. Continuous Electrodeposition for Lightweight, Highly Conducting and Strong Carbon Nanotube-Copper Composite Fibers. *Nanoscale* **2011**, *3*, 4215–4219.

For TOC only

Electroless Cu
Deposition

40